mater.scichina.com link.springer.com

Published online 24 June 2020 | https://doi.org/10.1007/s40843-020-1354-2
Sci China Mater 2020, 63(8): 1560–1569

SPECIAL ISSUE: Optical Gain Materials towards Enhanced Light-Matter Interactions

Self-assembly $In_2Se_3/SnSe_2$ heterostructure array with suppressed dark current and enhanced photosensitivity for weak signal

Zhaoqiang Zheng[1,2], Peifeng Chen[1], Jianting Lu[1], Jiandong Yao[3*], Yu Zhao[1], Menglong Zhang[4], Mingming Hao[1] and Jingbo Li[4,5*]

ABSTRACT **Functional van der Waals (vdWs) heterostructures based on layered materials have shown tremendous potential in next-generation optoelectronic devices. To date, numerous vdWs heterostructures have been investigated based on stacking or epitaxial growth technology. However, the complicated synthesis process greatly limits the large-scale integration of the heterostructure device array, which is essential for practical applications. Here, a planar photodetector array with an out-of-plane vertical $In_2Se_3/SnSe_2$ heterostructure as the photosensitive channel was self-assembled through a pulsed laser deposition (PLD) technique. The vertical built-in field was exploited to suppress the dark current and separate the photogenerated carriers. The realized devices possess an ultralow dark current of 6.3 pA, combined with a high detectivity of 8.8×10^{11} Jones and a high signal-to-noise ratio (SNR) beyond 3×10^4. These performance metrics not only are one order of magnitude superior to pure In_2Se_3 device, but also demonstrate the unique advantage of detecting weak signals. In addition, this heterostructure photodetector array can further be constructed on flexible polyimide (PI) substrate. These flexible devices also demonstrate effective light detection capability and the photoresponse remains unchanged even after 200 cycles of bending. These findings pave a way toward the development of next-generation large area and high integration optoelectronic technologies.**

Keywords: 2D material, photodetector, pulsed-laser deposition, van der Waals heterostructure

INTRODUCTION

In recent years, van der Waals (vdWs) layered materials have been widely studied due to their unique physical properties, such as strong light absorption, high carrier mobility and mechanical flexibility [1–3]. In particular, layered materials can circumvent the lattice matching constraints and thus they can flexibly combine to construct various vdWs heterostructures with tunable band alignment and atomically sharp interfaces, offering innovative avenues for implementing next-generation optoelectronics [4–8]. Motivated by this, numerous vdWs heterostructures have been assembled through mechanical stacking or vdWs epitaxial technology [9–11]. Lee *et al.* [12] reported an atomically thin vdWs heterostructure assembled from single or multiple layers of n-MoS_2 and p-WSe_2, which demonstrated a gate-tunable photovoltaic response with an external quantum efficiency (EQE) up to 34%. Other vdWs heterostructures, such as $PdSe_2/MoS_2$ [13], black phosphorus/InSe [6], WSe_2/SnS_2 [14], $MoTe_2/MoS_2$ [15], MoS_2/WS_2 [16] and $GaTe/MoS_2$ [17] have also been exploited in solar cells or photodetectors. By virtue of the dangling-bond-free interface that allows the photoexcited carriers to travel efficiently across the interfacial layer [18,19], devices based on these vdWs heterostructures exhibit high performance. Nevertheless, some drawbacks have to be overcome for practice application. As to the mechanical stacking method, it depends

[1] School of Materials and Energy, Guangdong University of Technology, Guangzhou 510006, China
[2] Department of Electronic Engineering, the Chinese University of Hong Kong, Hong Kong, China
[3] State Key Laboratory of Optoelectronic Materials and Technologies, Nanotechnology Research Center, School of Materials Science & Engineering, Sun Yat-sen University, Guangzhou 510275, China
[4] Institute of Semiconductors, South China Normal University, Guangzhou 510631, China
[5] State Key Laboratory for Superlattices and Microstructures, Institute of Semiconductors, Chinese Academy of Sciences, Beijing 100083, China
* Corresponding authors (emails: yaojd@mail2.sysu.edu.cn (Yao J); jbli@semi.ac.cn (Li J))

on the possibility of cleaving bulk crystal. The size of the mechanically exfoliated layered materials is small, and the complicated transfer processes inevitably introduce interface defects, which hinder their applications in highly integrated devices [20]. As to the vdWs epitaxial method, it can directly synthesize heterostructures with high crystallinity and clean interface [3,7,21]. These vdWs heterostructures have made pioneering advances in the fields of field-effect transistors, light-emitting diodes and photodetectors [22–24]. Despite these progresses, the vdWs epitaxial process involves high temperature and inevitably produces residues. They are critical hurdles for large-scale integration of vdWs heterostructure array with controlled spatial position and structure, especially on flexible substrates [4].

Recently, pulsed laser deposition (PLD), a versatile growth technique, has been adopted for the preparation of high-quality layered materials [25–27]. PLD is a clean and scalable physical vapor deposition process, which can fabricate centimeter-scale layered material films. Additionally, the PLD process is facile and compatible with flexible substrates [28]. Meanwhile, the thickness and geometry of the PLD-grown layered materials are easy to control [29]. Thus, PLD holds great potential to yield high-quality heterostructures and manufacture scalable integrated devices.

In this work, photodetector array based on $In_2Se_3/SnSe_2$ heterostructures was realized by using a self-assembled PLD method. The geometry and alignment of the In_2Se_3 and $SnSe_2$ films can be controlled through a mask, which is free from any transfer or other patterning steps, resulting in outstanding heterostructure characteristic. The realized devices possess an ultralow dark current of 6.3 pA, combined with a high detectivity of 8.8×10^{11} Jones, a short rise/fall time of 3.4/3.7 ms and a high signal-to-noise ratio (SNR) beyond 3×10^{4}. These figures-of-merit indicate that the $In_2Se_3/SnSe_2$ heterostructures hold unique advantages for weak signal detection. We further applied these $In_2Se_3/SnSe_2$ heterostructures for flexible photodetectors, which also demonstrated effective light detection capability and stability. This study depicts a fascinating landscape for the further development of large-area optoelectronics.

EXPERIMENTAL SECTION

Self-assembly of the $In_2Se_3/SnSe_2$ photodetector array

As schematic shown in Fig. 1, we firstly adopted acetone, alcohol and deionized water to clean the commercially purchased SiO_2/Si and polyimide (PI) substrates. Then, 5-μm-spaced Ti/Au (60/10 nm) electrode array was patterned onto the substrates by a photolithography process (μpg 501, Heidelberg) and deposited by electron beam evaporation. Secondly, the electrode array was coved by a stainless-steel mask, and the In_2Se_3 and $SnSe_2$ films were synthesized by PLD (COM-PexPro 201, Coherent). The experimental parameters were as follows. The deposition chamber was evacuated to 2×10^{-4} Pa, and then Ar gas (99.999%) was guided into the chamber at the rate of 50 sccm. For depositing In_2Se_3, the working temperature

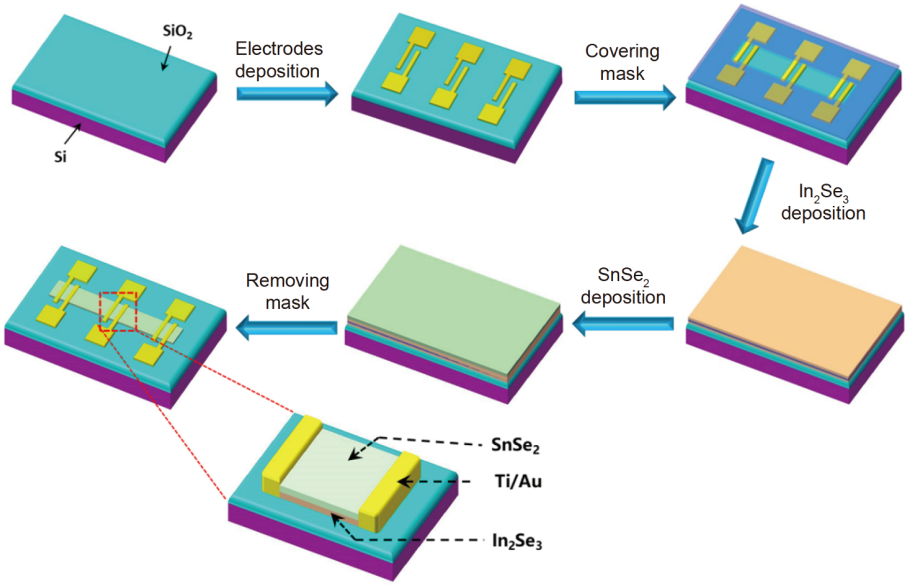

Figure 1 Schematic diagram of the construction process of the $In_2Se_3/SnSe_2$ photodetector array.

and working pressure were 420°C and 20 Pa, respectively. The frequency and power of the pulsed laser were 4 Hz and 105 mJ per pulse, respectively. The total pulse number was 1200. For depositing $SnSe_2$, the working temperature and working pressure were 340°C and 30 Pa, respectively. The frequency and power of the pulsed laser were 4 Hz and 120 mJ per pulse, respectively. The total pulse numbers were 600, 1200 and 1600, respectively. Finally, the samples were annealed in the chamber at 200°C for 30 min and the mask was removed.

Characterization of the $In_2Se_3/SnSe_2$ heterostructure

The surface topography and thickness of the $In_2Se_3/SnSe_2$ film were obtained through scanning electron microscopy (SEM; SU8220, Hitach, Japan) and atomic force microscopy (AFM; Dimension FastScan, Bruker, Germany) systems. Crystallinity of the heterostructure was confirmed by X-ray diffraction (XRD; D8 ADVANCE, Bruker). Raman spectra were measured by using a HORIBA LabRAM Raman confocal microscope (Japan) under a 532-nm laser excitation. Compositions and energy band structures of the samples were evaluated by Thermo Fisher Escalab 250Xi (USA) under the X-ray photoelectron spectroscopy (XPS) and ultraviolet photoelectron spectroscopy (UPS) modes, respectively. Vis-NIR absorption spectrum was recorded through a Perkin Elmer spectrophotometer (Lambda 950, USA).

Optoelectronic measurement of the devices

The optoelectrical properties were investigated through a Lakeshore probe station connected to the Keithley semiconductor analyzer (4200-SCS) under ambient condition. A semiconductor laser with wavelength of 447 nm was used as the incident light source. The spot radius was 10 mm, and we adopted a Throlabs silicon photodiode (S120VC) to measure the incident light power. For characterizing the stability and response speed, pulsed light was modulated by a chopper. A home-built measurement system was used to measure the response speed under the pulsed light. A Tektronix oscilloscope (DPO 4102B) was employed to record the temporal photocurrent.

RESULTS AND DISCUSSION

The schematic of the self-assembly process for the $In_2Se_3/SnSe_2$ heterostructure array is shown in Fig. 1. The detailed instructions are described in the Experimental Section. The device architecture of an individual $In_2Se_3/SnSe_2$ photodetector contains an out-of-plane vertical $In_2Se_3/SnSe_2$ heterostructure as the photosensitive channel, and symmetric Ti/Au (60/10 nm) electrodes were selected to achieve Ohmic contact with the heterostructure. Fig. 2a presents a typical SEM image of the deposited In_2Se_3 film. Sheet-like compact and continuous polycrystalline morphologies have been observed. The

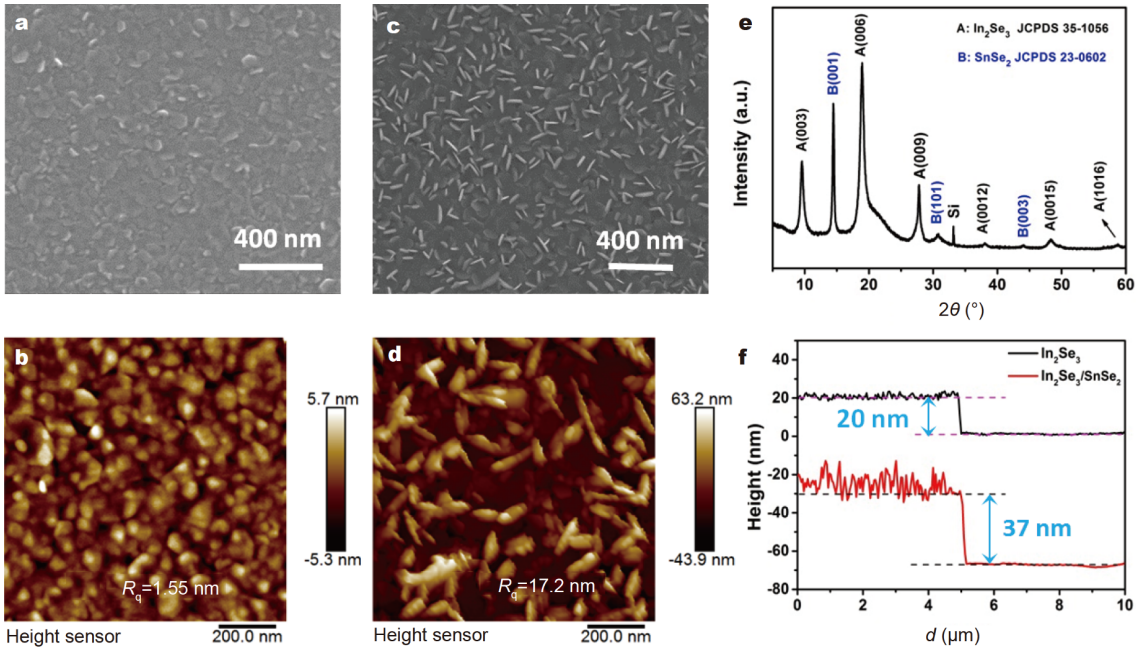

Figure 2 Morphology and structure characterizations of the fabricated $In_2Se_3/SnSe_2$ heterostructure. (a) SEM image and (b) AFM image of the In_2Se_3 film. (c) SEM image and (d) AFM image of the $In_2Se_3/SnSe_2$ heterostructure. (e) XRD pattern of the $In_2Se_3/SnSe_2$ heterostructure. (f) AFM height profiles across the edges of the In_2Se_3 and $In_2Se_3/SnSe_2$ films.

film is uniform and flat, indicating laterally aligned In_2Se_3, which is well compatible with other layered materials. AFM image of the In_2Se_3 film is shown in Fig. 2b. The root-mean-square (RMS) roughness of the In_2Se_3 film is about 1.55 nm, confirming a smooth surface. Raman spectrum of the as-synthesized In_2Se_3 film is shown in Fig. S1. The vibration peaks match well with the features of β-phase In_2Se_3 [30]. Then, to investigate the valence states of constituent elements, XPS measurements were performed. The XPS spectrum of the whole range scanning (Fig. S2a) shows that only In and Se elements are present, indicating high purity of the sample. High-resolution XPS spectra of the In 3d and Se 3d are presented in Fig. S2b and c, respectively. The peaks centered at 452.6 and 445.1 eV can be assigned to the In $3d_{3/2}$ and In $3d_{5/2}$ binding characteristics of In_2Se_3, respectively [31]. Deconvolution analysis of the XPS spectrum of Se 3d reveals two split peaks, located at 54.3 and 53.5 eV, which can be assigned to Se $3d_{3/2}$ and Se $3d_{5/2}$ binding characteristics of In_2Se_3, respectively [31]. The calculated atomic molar ratio of Se/In in the film is 2.9/2, roughly consistent with the stoichiometric ratio of 3/2, indicating the high quality of In_2Se_3 film. Fig. 2c shows a typical SEM image of the $In_2Se_3/SnSe_2$ heterostructure. As can be seen, except a smooth background, vertically oriented $SnSe_2$ layers uniformly distribute on the heterostructure. These vertically aligned $SnSe_2$ nanosheets enhance the surface area, which is beneficial for light trapping. AFM image of the heterostructure is presented in Fig. 2d. After the deposition of $SnSe_2$, the film becomes rather rough with an RMS up to 17.2 nm. Raman spectrum of the $In_2Se_3/SnSe_2$ heterostructure is provided in Fig. S1. The in-plane vibration mode (E_g) and out-of-plane vibration mode (A_{1g}) are observed at 120 and 188 cm^{-1}, respectively, confirming the formation of 1T-phase $SnSe_2$ [32]. In addition, the characteristic peaks of In_2Se_3 well remain after the deposition of $SnSe_2$, revealing that the deposition of $SnSe_2$ will induce negligible structural damage to the In_2Se_3 film. Then, XPS analysis of the $SnSe_2$ in Fig. S3 demonstrates that the prepared $SnSe_2$ is also of high quality.

To further investigate the crystal structures of the PLD-grown $In_2Se_3/SnSe_2$ heterostructure, XRD measurement was performed. Fig. 2e presents the XRD pattern of the heterostructure. These diffraction peaks can be well assigned to 1T-phase $SnSe_2$ (JCPDS 23-0602) and β-phase In_2Se_3 (JCPDS 35-1056). These sharp peaks reveal the high crystallinity of $SnSe_2$ and In_2Se_3. Additionally, as indexed in the labels, the In_2Se_3 exhibits only the (003) family diffraction peaks, indicating its *c*-axis oriented characteristic. In other words, the In_2Se_3 layers are stacked out-of-plane through vdWs interaction and end on the surface without dangling bonds, so it shows a smooth surface. As to $SnSe_2$, the main diffraction peak is (001), which indicates that the smooth $SnSe_2$ is also *c*-axis oriented. According to previous reports [33,34], for layered materials, the in-plane transport efficiency of carrier is several orders of magnitude higher than the out-of-plane transport. Therefore, these highly oriented characteristics of In_2Se_3 and $SnSe_2$ have laid a solid foundation for the construction of high-performance planar photodetectors.

Then, AFM measurements were performed at the edge of the heterostructure to detect the thickness. As shown in Fig. 2f, the height profiles reveal that the thicknesses of the In_2Se_3 and the $In_2Se_3/SnSe_2$ heterostructure are 20 and 37 nm (excluding vertically oriented $SnSe_2$), respectively. Thus, the thickness of flat $SnSe_2$ is deduced to be 17 nm. For PLD technology, the thickness of the films can be precisely controlled by the number of laser pulses [35]. According to a previous report [31], ~20 nm In_2Se_3 has demonstrated the superiority for photodetection. Thus, we deposited a 20 nm In_2Se_3 film and deposited $SnSe_2$ films with different thicknesses. As shown in Fig. S4, as the thickness of the $SnSe_2$ film increases, the RMS of the film increases. When the thickness exceeds 17 nm, the RMS slightly decreases and the surface topography changes.

Then, photoresponse performances of the constructed photodetectors (pure In_2Se_3, pure $SnSe_2$ and $In_2Se_3/SnSe_2$ heterostructures) were investigated and compared. Fig. 3a and Fig. S5 show the current-voltage (*I*-*V*) curves of the devices measured in dark and under 447 nm light irradiation with a light intensity of 23.7 mW cm^{-2}. We can see that the pure In_2Se_3 (Fig. 3a1) and $SnSe_2$ (Fig. S5a) devices present relatively large dark currents (I_{dark}) of ~78 and 264 pA, respectively. After deposition of the $SnSe_2$ films on In_2Se_3, the dark current was effectively suppressed. With only 10 nm $SnSe_2$ film deposited, the dark current was reduced to ~42 pA (Fig. 3a2). When the thickness of the $SnSe_2$ film was increased to 17 nm, the dark current was further reduced to 6.3 pA (Fig. 3a3), which was one order of magnitude lower than the pure In_2Se_3 device. Meanwhile, as the thickness of the deposited $SnSe_2$ film increased, the photocurrent (I_{ph}, $I_{ph}=I_{light}-I_{dark}$, I_{light} is the channel current upon illumination) of the device also increased significantly (Figs S5b and S6). However, when the $SnSe_2$ film was increased from 17 to 22 nm, the dark current began to increase instead (Fig. 3a4). At the same time, compared with the 17 nm

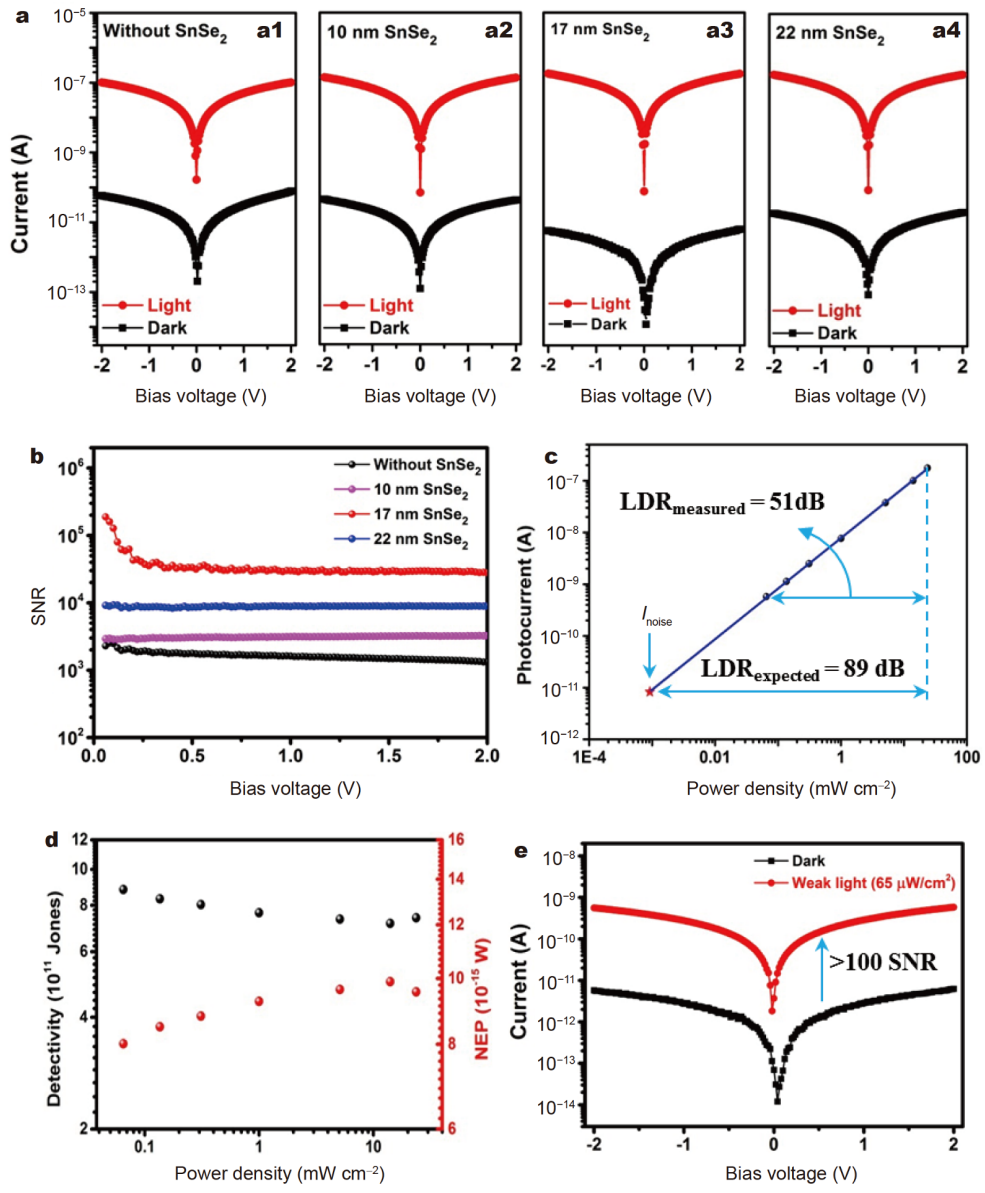

Figure 3 Photoresponse of the $In_2Se_3/SnSe_2$ devices. (a) *I-V* curves of the photodetectors with different $SnSe_2$ thicknesses. (b) Bias dependence of the SNR calculated on the constructed devices. (c) Photocurrent of the $In_2Se_3/SnSe_2$ device under various light intensities at V_{ds}=2 V. Due to instrument limitations, the measured LDR is 51 dB. Calculated noise current is marked by an asterisk, and the expected LDR is 89 dB. (d) Measured detectivity (black) and NEP (red) of the $In_2Se_3/SnSe_2$ device under different light intensities. (e) *I-V* curves of the $In_2Se_3/SnSe_2$ device in dark and under illumination of weak light (65 μW cm^{-2}).

$SnSe_2$ device, the photocurrent just slightly increased (Fig. S6).

For evaluating the weak-light detection capability of photodetectors, SNR is a crucial performance metric. It is defined as [36]

$$\mathrm{SNR} = I_{\mathrm{ph}} / I_{\mathrm{dark}}. \quad (1)$$

In the photodetection process, noise always exists and will generate random fluctuations in the device's output, thereby limiting the detection of weak signal. Higher SNR means weaker disturbances from the background noise [37]. Fig. 3b shows the SNR *versus* bias voltage of the constructed devices. The $In_2Se_3/SnSe_2$ heterostructure device with 17 nm $SnSe_2$ shows a high SNR beyond 3×10^4, which is significantly larger than the other devices. It turns out that 17 nm is the optimum thickness of the $SnSe_2$ film for our devices. Therefore, in this work, our attention focuses on the $In_2Se_3/SnSe_2$ photodetector with

17 nm $SnSe_2$ film.

Figs S5c and S7 present the *I-V* curves of the pure $SnSe_2$ and the heterostructure devices in linear coordinates in the dark. The symmetric and linear *I-V* curves indicate Ohmic-like contacts between the active film and Ti/Au electrodes. Fig. 3c shows the photocurrent *versus* light intensity at the bias voltage (V_{ds}) of 2 V. The photocurrent increases linearly with increasing irradiation power. Linear dynamic range (LDR) is a performance metric used to characterize the power range of a photodetector with linear optical signal [38,39]. Large LDR is required in high contrast applications. Commonly, the LDR is expressed as

$$\mathrm{LDR} = 20\log\left(P_{\mathrm{upper}} / P_{\mathrm{lower}}\right), \tag{2}$$

where P_{upper} and P_{lower} are the input light power upper and lower limits where the linear response is observed [38]. Fig. 3c presents a linear response from 0.065 to 23.7 mW cm^{-2}, corresponding to an LDR of 51 dB. The minimal and maximum light intensities in Fig. 3c were determined by the output limitations of the laser that we used. In order to obtain the actual LDR more accurately, a noise current, which corresponds to the photocurrent for SNR to be unity, was adopted to further calculate the LDR value [39]. Thus, we get an expected LDR value of 89 dB, which corresponds to a minimum detection optical signal down to ~0.8 μW cm^{-2}.

Detectivity (D^*) is another useful performance metric to evaluate the capability of a photodetector to detect weak optical signals [18]. D^* is defined as [39]

$$D^* = (Af)^{1/2} / \mathrm{NEP}, \tag{3}$$

where A is the effective area of the device (5 μm× 1000 μm), f is the bandwidth, and NEP denotes the noise equivalent power. Commonly, we assume that the shot noise from dark current is the dominant contribution [40,41]. Consequently, the NEP and D^* can be expressed by

$$\mathrm{NEP} = \left[PA(2eI_{\mathrm{dark}})^{1/2}\right] / I_{\mathrm{ph}}, \tag{4}$$

$$D^* = A^{1/2} I_{\mathrm{ph}} / \left[PA(2eI_{\mathrm{dark}})^{1/2}\right], \tag{5}$$

where P and e are the light density and electronic charge, respectively. Fig. 3d shows the NEP and D^* *versus* light intensity. It is seen that our device exhibits a low NEP less than 10^{-14} W $Hz^{-1/2}$, giving rise to a high D^* of 8.8×10^{11} Jones. These NEP and D^* values are comparable to those of commercial Si-based photodetectors (~10^{-14} W $Hz^{-1/2}$, ~10^{12} Jones) [18], and they are better than most of the previously reported values for vdWs material-based and perovskite-based photodetectors [34,39,42–45]. Next, to further evaluate the weak light detection ability, *I-V* curves of the $In_2Se_3/SnSe_2$ device in dark and under weak light illumination were displayed in Fig. 3e. Obviously, even if the incident light was as weak as 65 μW cm^{-2}, which was less than 1/1000 of 1 sun (100 mW cm^{-2}), the SNR was still larger than 100 (Fig. S8).

Responsivity (R) and EQE are important figures-of-merit for evaluating the performance of photodetectors. They can be calculated by using the following formulas:

$$R = I_{\mathrm{ph}} / PA, \tag{6}$$

$$\mathrm{EQE} = hcR / (e\lambda) \times 100\%, \tag{7}$$

where h is the Planck constant, λ is the incident wavelength and c is the velocity of light [46,47]. We obtained the R and EQE to be 177 mA W^{-1} and 49.2%, respectively.

Long-term device stability and fast response to incident light are also important for high-performance photodetectors. In the following step, we performed time-resolved photoresponse experiments through periodically turning on and off the incident laser. As presented in Fig. 4a, the current on/off switching was rapid and reproducible for 500 cycles. Meanwhile, the photoresponse changed little (<2%) over the entire test period, indicating that the device was stable and reliable. Then, as presented in Fig. 4b, the temporal response of one photoswitching cycle was recorded through an oscilloscope. The rise time (τ_r) and decay time (τ_d) can be calculated through fitting the rising and falling edges of the response current with the following single exponential function [42]:

$$I(t) = I_{\mathrm{d}} + C\exp\left(t / \tau_{\mathrm{r}} \text{ or } \tau_{\mathrm{d}}\right), \tag{8}$$

where C is a scaling constant. In Fig. 4b, we obtained τ_r and τ_d of 3.4 and 3.7 ms, respectively. These values are relatively fast compared with the state-of-the-art vdWs material-based photoconductive devices [13,48]. Table S1 summarizes the performance metrics of different materials-based photodetectors. Importantly, in the comprehensive consideration of the overall performances, our $In_2Se_3/SnSe_2$ device stands out, indicating its superiority for weak light detection application. In the following step, we performed optoelectronic measurements for other devices on the chip. As demonstrated in Fig. 4c, there are seven photodetectors in a chip, and the variation of detectivity among devices is small. This result reveals that the constructed $In_2Se_3/SnSe_2$ device array has satisfactory uniformity, showing high potential for imaging applications.

Sequentially, energy band structures of the hetero-

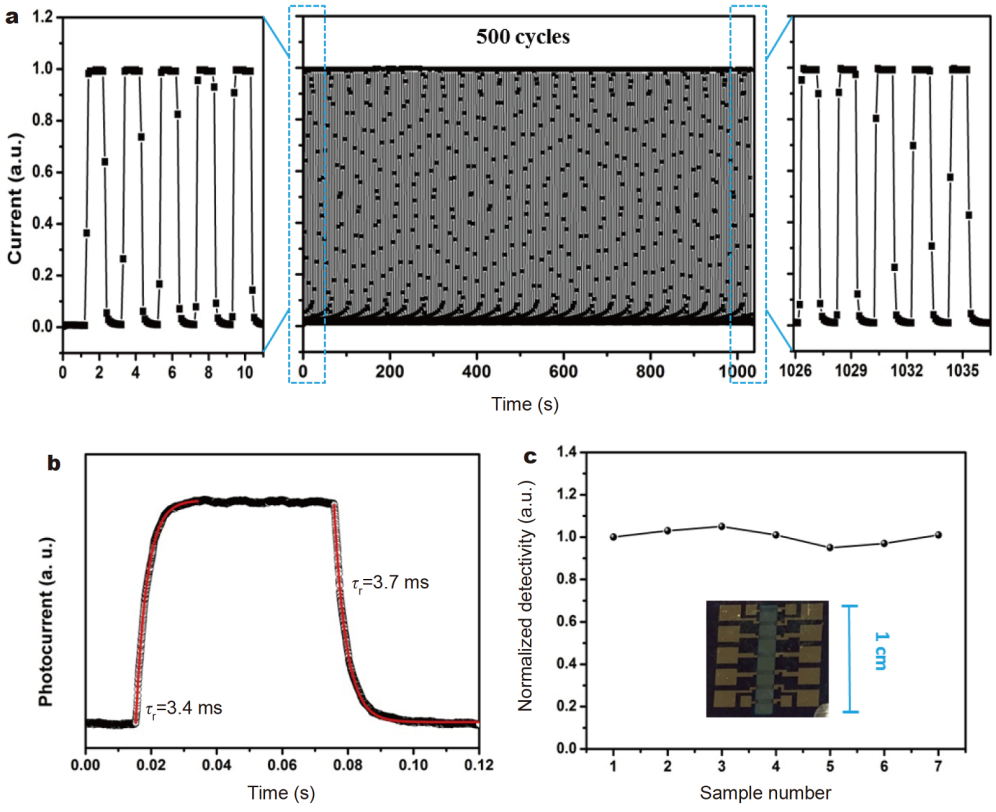

Figure 4 (a) Normalized photoswitching evolution of the $In_2Se_3/SnSe_2$ device under periodic light irradiation (65 μW cm^{-2}). The left and right parts present the magnified details of the curves at the first and last five cycles. (b) Rising and falling curves of the $In_2Se_3/SnSe_2$ device obtained through an oscilloscope. The curves are fitted with a single exponential function. (c) Normalized distribution of the detectivities of seven heterostructure devices. Inset shows the optical image of the device array.

structure were investigated to unveil the synergistic effect between In_2Se_3 and $SnSe_2$. UPS spectra around the cutoff and onset edges of the $SnSe_2$ are presented in Fig. 5a and b , respectively. Through extrapolating their leading edges linearly and finding the intersections with the baselines, the work function of the $SnSe_2$ film can be calculated to be 4.61 eV (21.22−16.61=4.61 eV), and the valence band maximum (E_v) is 0.71 eV below the Fermi level (E_f). Fig. 5c shows the Vis-NIR absorption spectrum of the $SnSe_2$ film. Given multilayer $SnSe_2$ is an indirect bandgap semiconductor [42], the corresponding Tauc plot is shown in the inset of Fig. 5c. A bandgap of 1.13 eV, which matches well with previous reports [42,49], is extracted from the plot. Thus, the energy level of conduction band minimum (E_C) was calculated to be −4.19 eV. Combining the band structure of In_2Se_3 that has been determined in previous study [31], we sketched the band structure diagram of the $In_2Se_3/SnSe_2$ heterostructure in Fig. 5d. In this bandgap model, the enhanced photodetection performance can be explained as follows: on one hand, the depletion region is formed at the interface of In_2Se_3 and $SnSe_2$ (Fig. 5d), which brings about a narrowed conducting channel in the heterostructure and thus greatly suppresses the dark current; when $SnSe_2$ is thin, it is completely depleted. As the thickness of $SnSe_2$ increases, the depletion region gradually expands, narrowing the conductive channel and decreasing the dark current. When the thickness of $SnSe_2$ exceeds 17 nm, In_2Se_3 is completely depleted. Thus, as the thickness of $SnSe_2$ increases, carriers can flow through the $SnSe_2$ film, increasing the dark current. On the other hand, this type-II staggered band alignment is beneficial to the dissociation of photoexcited carriers (Fig. 5e), which significantly reduces their recombination, resulting in a high photocurrent.

Finally, the $In_2Se_3/SnSe_2$ heterostructure can also be deposited on the PI substrate to construct the flexible photodetector array. We also investigated the photoresponse property of these flexible devices. Fig. 6a shows the *I-V* curves of a typical flexible device in dark and

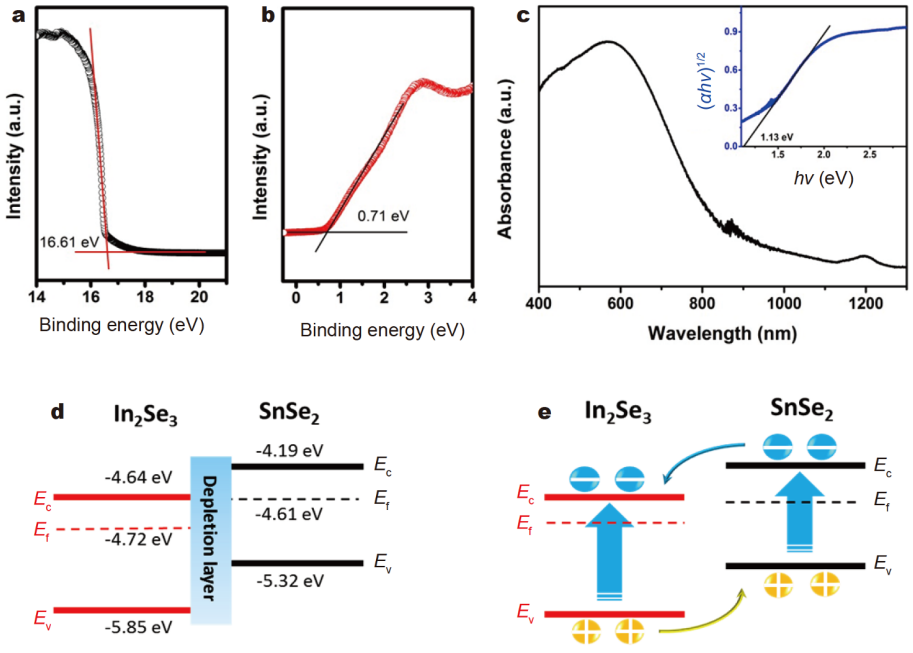

Figure 5 UPS spectra around the (a) low energy cutoff region and (b) onset region of the $SnSe_2$. (c) Vis-NIR absorption spectrum of the $SnSe_2$ and the corresponding Tauc plot. (d) Energy band diagrams of In_2Se_3 and $SnSe_2$. (e) Photoexcited carrier transport process in the $In_2Se_3/SnSe_2$ heterostructure.

under 447 nm light irradiation. Clearly, this device also exhibits outstanding photodetection capability. Then, detailed device parameters were calculated and listed in Table S2. It can be observed that the performance of this flexible photodetector is comparable to that of the devices on rigid SiO_2/Si substrate. Next, we performed rough flexibility tests, in which the device was bent to an angle of ~60° (Fig. S9) for different cycles. Fig. 6b and Fig. S10 compare the *I*-*V* curves of this flexible device before and after bending for various cycles. Obviously, whether in dark or under irradiation, the conductance of this device remains almost constant over 200 cycles, indicating its excellent flexibility. Fig. S11 presents the detectivity distribution of the flexible photodetector array. There are also seven devices on a chip, and the performance of these devices also manifests satisfactory uniformity. Such a result reveals that PLD technology manifests extensive compatibility with various substrates, which provides a bright future for advanced optoelectronic applications.

CONCLUSIONS

In summary, a vertical $In_2Se_3/SnSe_2$ heterostructure photodetector array was designed and self-assembled through a facile PLD approach. In such heterostructure

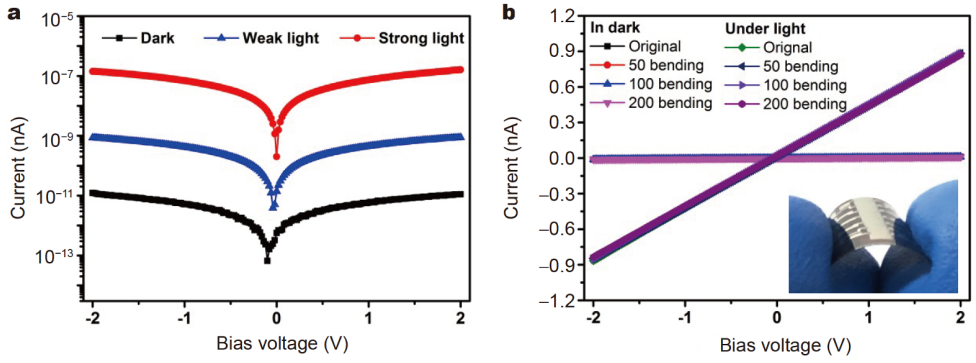

Figure 6 Photoresponse of the constructed $In_2Se_3/SnSe_2$ photodetector array on the flexible PI substrate. (a) *I*-*V* curves of a typical flexible device in dark, under illumination of weak light (65 μW cm^{-2}) and strong light (23.7 mW cm^{-2}). (b) *I*-*V* curves of the flexible device upon various bending cycles. Inset shows a photograph of the bended $In_2Se_3/SnSe_2$ photodetector array. The light intensity is 65 μW cm^{-2}.

devices, the dark current was significantly suppressed owing to the formation of depletion region. Upon light irradiation, photoexcited carriers were spatially separated and their recombination rate was reduced, leading to enhanced photocurrent. These heterostructure devices greatly outperform the pure In_2Se_3 device and show ultralow dark current of 6.3 pA, high detectivity of 8.8×10^{11} Jones, short rise/fall time of 3.4/3.7 ms and high SNR beyond 3×10^4. These performance metrics indicate that the $In_2Se_3/SnSe_2$ heterostructures hold unique advantages for the detection of weak signals. Additionally, the $In_2Se_3/SnSe_2$ photodetector array constructed on the flexible PI substrate presents comparable performance to that on SiO_2/Si substrate, revealing the great potential for future wearable optoelectronics.

Received 28 February 2020; accepted 14 April 2020; published online 24 June 2020

1 Cai Z, Liu B, Zou X, *et al.* Chemical vapor deposition growth and applications of two-dimensional materials and their heterostructures. Chem Rev, 2018, 118: 6091–6133
2 Wang F, Wang Z, Yin L, *et al.* 2D library beyond graphene and transition metal dichalcogenides: A focus on photodetection. Chem Soc Rev, 2018, 47: 6296–6341
3 Yang T, Zheng B, Wang Z, *et al.* Van der Waals epitaxial growth and optoelectronics of large-scale WSe_2/SnS_2 vertical bilayer p-n junctions. Nat Commun, 2017, 8: 1906
4 Lee JB, Lim YR, Katiyar AK, *et al.* Direct synthesis of a self-assembled WSe_2/MoS_2 heterostructure array and its optoelectrical properties. Adv Mater, 2019, 31: 1904194
5 Liu H, Zhu X, Sun X, *et al.* Self-powered broad-band photodetectors based on vertically stacked WSe_2/Bi_2Te_3 p-n heterojunctions. ACS Nano, 2019, 13: 13573–13580
6 Zhao S, Wu J, Jin K, *et al.* Highly polarized and fast photoresponse of black phosphorus-InSe vertical p-n heterojunctions. Adv Funct Mater, 2018, 28: 1802011
7 Zhang Z, Chen P, Duan X, *et al.* Robust epitaxial growth of two-dimensional heterostructures, multiheterostructures, and superlattices. Science, 2017, 357: 788–792
8 Zheng Z, Yao J, Zhu L, *et al.* Tin dioxide quantum dots coupled with graphene for high-performance bulk-silicon Schottky photodetector. Mater Horiz, 2018, 5: 727–737
9 Tan H, Fan Y, Zhou Y, *et al.* Ultrathin 2D photodetectors utilizing chemical vapor deposition grown WS_2 with graphene electrodes. ACS Nano, 2016, 10: 7866–7873
10 Wu F, Li Q, Wang P, *et al.* High efficiency and fast van der Waals hetero-photodiodes with a unilateral depletion region. Nat Commun, 2019, 10: 4663
11 Lu J, Zheng Z, Yao J, *et al.* 2D In_2S_3 nanoflake coupled with graphene toward high-sensitivity and fast-response bulk-silicon schottky photodetector. Small, 2019, 15: 1904912
12 Lee CH, Lee GH, van der Zande AM, *et al.* Atomically thin p-n junctions with van der Waals heterointerfaces. Nat Nanotech, 2014, 9: 676–681
13 Long M, Wang Y, Wang P, *et al.* Palladium diselenide long-wavelength infrared photodetector with high sensitivity and stability. ACS Nano, 2019, 13: acsnano.8b09476
14 Zhou X, Hu X, Zhou S, *et al.* Tunneling diode based on WSe_2/SnS_2 heterostructure incorporating high detectivity and responsivity. Adv Mater, 2018, 30: 1703286
15 Ding Y, Zhou N, Gan L, *et al.* Stacking-mode confined growth of 2H-$MoTe_2/MoS_2$ bilayer heterostructures for UV-vis-IR photodetectors. Nano Energy, 2018, 49: 200–208
16 Murthy AA, Stanev TK, Cain JD, *et al.* Intrinsic transport in 2D heterostructures mediated through h-BN tunneling contacts. Nano Lett, 2018, 18: 2990–2998
17 Wang F, Wang Z, Xu K, *et al.* Tunable GaTe-MoS_2 van der Waals p-n junctions with novel optoelectronic performance. Nano Lett, 2015, 15: 7558–7566
18 Long M, Wang P, Fang H, *et al.* Progress, challenges, and opportunities for 2D material based photodetectors. Adv Funct Mater, 2018, 29: 1803807
19 Zhou X, Hu X, Yu J, *et al.* 2D layered material-based van der Waals heterostructures for optoelectronics. Adv Funct Mater, 2018, 28: 1706587
20 Tang Y, Wang Z, Wang P, *et al.* WSe_2 photovoltaic device based on intramolecular p-n junction. Small, 2019, 15: 1805545
21 Gong Y, Lin J, Wang X, *et al.* Vertical and in-plane heterostructures from WS_2/MoS_2 monolayers. Nat Mater, 2014, 13: 1135–1142
22 Withers F, Del Pozo-Zamudio O, Mishchenko A, *et al.* Light-emitting diodes by band-structure engineering in van der Waals heterostructures. Nat Mater, 2015, 14: 301–306
23 Duan X, Wang C, Shaw JC, *et al.* Lateral epitaxial growth of two-dimensional layered semiconductor heterojunctions. Nat Nanotech, 2014, 9: 1024–1030
24 Zhang Y, Yin L, Chu J, *et al.* Edge-epitaxial growth of 2D NbS_2-WS_2 lateral metal-semiconductor heterostructures. Adv Mater, 2018, 30: 1803665
25 Zheng Z, Yao J, Yang G. Centimeter-scale deposition of $Mo_{0.5}W_{0.5}Se_2$ alloy film for high-performance photodetectors on versatile substrates. ACS Appl Mater Interfaces, 2017, 9: 14920–14928
26 Zheng Z, Yao J, Yang G. Self-assembly of the lateral $In_2Se_3/CuInSe_2$ heterojunction for enhanced photodetection. ACS Appl Mater Interfaces, 2017, 9: 7288–7296
27 Zheng Z, Yao J, Xiao J, *et al.* Synergistic effect of hybrid multilayer In_2Se_3 and nanodiamonds for highly sensitive photodetectors. ACS Appl Mater Interfaces, 2016, 8: 20200–20211
28 Yao JD, Zheng ZQ, Yang GW. Production of large-area 2D materials for high-performance photodetectors by pulsed-laser deposition. Prog Mater Sci, 2019, 106: 100573
29 Yao J, Zheng Z, Yang G. Ultrasensitive 2D/3D heterojunction multicolor photodetectors: A synergy of laterally and vertically aligned 2D layered materials. ACS Appl Mater Interfaces, 2018, 10: 38166–38172
30 Zheng ZQ, Yao JD, Yang GW. Growth of centimeter-scale high-quality In_2Se_3 films for transparent, flexible and high performance photodetectors. J Mater Chem C, 2016, 4: 8094–8103
31 Zheng Z, Yao J, Wang B, *et al.* Self-assembly high-performance UV-vis-NIR broadband β-In_2Se_3/Si photodetector array for weak signal detection. ACS Appl Mater Interfaces, 2017, 9: 43830–43837
32 Gao W, Zheng Z, Li Y, *et al.* High performance tin diselenide photodetectors dependent on thickness: A vertical graphene sandwiched device and interfacial mechanism. Nanoscale, 2019, 11: 13309–13317

33 Peng H, Xie C, Schoen DT, *et al.* Large anisotropy of electrical properties in layer-structured In_2Se_3 nanowires. Nano Lett, 2008, 8: 1511–1516
34 Yao J, Yang G. Flexible and high-performance all-2D photodetector for wearable devices. Small, 2018, 14: 1704524
35 Lu Z, Xu Y, Yu Y, *et al.* Ultrahigh speed and broadband few-layer $MoTe_2$/Si 2D-3D heterojunction-based photodiodes fabricated by pulsed laser deposition. Adv Funct Mater, 2020, 30: 1907951
36 Xie C, Mak C, Tao X, *et al.* Photodetectors based on two-dimensional layered materials beyond graphene. Adv Funct Mater, 2016, 27: 1603886
37 Ren Z, Sun J, Li H, *et al.* Bilayer PbS quantum dots for high-performance photodetectors. Adv Mater, 2017, 29: 1702055
38 Zeng J, Meng C, Li X, *et al.* Interfacial-tunneling-effect-enhanced $CsPbBr_3$ photodetectors featuring high detectivity and stability. Adv Funct Mater, 2019, 29: 1904461
39 Deng W, Zhang X, Huang L, *et al.* Aligned single-crystalline perovskite microwire arrays for high-performance flexible image sensors with long-term stability. Adv Mater, 2016, 28: 2201–2208
40 Fu Q, Zhu C, Zhao X, *et al.* Ultrasensitive 2D Bi_2O_2Se phototransistors on silicon substrates. Adv Mater, 2019, 31: 1804945
41 Ma C, Shi Y, Hu W, *et al.* Heterostructured $WS_2/CH_3NH_3PbI_3$ photoconductors with suppressed dark current and enhanced photodetectivity. Adv Mater, 2016, 28: 3683–3689
42 Zhou X, Gan L, Tian W, *et al.* Ultrathin $SnSe_2$ flakes grown by chemical vapor deposition for high-performance photodetectors. Adv Mater, 2015, 27: 8035–8041
43 Ou Q, Zhang Y, Wang Z, *et al.* Strong depletion in hybrid perovskite p-n junctions induced by local electronic doping. Adv Mater, 2018, 30: 1705792
44 Zhou X, Hu X, Zhou S, *et al.* Ultrathin 2D $GeSe_2$ rhombic flakes with high anisotropy realized by van der Waals epitaxy. Adv Funct Mater, 2017, 27: 1703858
45 Lu J, Zheng Z, Gao W, *et al.* Epitaxial growth of large-scale In_2S_3 nanoflakes and the construction of a high performance In_2S_3/Si photodetector. J Mater Chem C, 2019, 7: 12104–12113
46 Zheng Z, Zhang T, Yao J, *et al.* Flexible, transparent and ultra-broadband photodetector based on large-area WSe_2 film for wearable devices. Nanotechnology, 2016, 27: 225501
47 Gao W, Zheng Z, Huang L, *et al.* Self-powered $SnS_{1-x}Se_x$ alloy/silicon heterojunction photodetectors with high sensitivity in a wide spectral range. ACS Appl Mater Interfaces, 2019, 11: 40222–40231
48 Gong C, Chu J, Yin C, *et al.* Self-confined growth of ultrathin 2D nonlayered wide-bandgap semiconductor CuBr flakes. Adv Mater, 2019, 31: 1903580
49 Perumal P, Ulaganathan RK, Sankar R, *et al.* Ultra-thin layered ternary single crystals $[Sn(S_x\ Se_{1-x})_2]$ with bandgap engineering for high performance phototransistors on versatile substrates. Adv Funct Mater, 2016, 26: 3630–3638

Acknowledgements This work was supported by the National Natural Science Foundation of China (61805044 and 11674310), the Key Platforms and Research Projects of Department of Education of Guangdong Province (2018KTSCX050), and "The Pearl River Talent Recruitment Program". We thank the Analysis and Test Center, Guangdong University of Technology for the topography and microanalysis of our specimens.

Author contributions Yao J and Li J designed the project and the experiments; Zheng Z carried out the main experiments and wrote this manuscript; Chen P and Lu J completed the rest of the experiments and helped write this manuscript; the other authors helped to analyze the data, discussed the results and contributed to the theoretical analysis.

Conflict of interest The authors declare that they have no conflict of interest.

Supplementary information Experimental details and supporting data are available in the online version of the paper.

Zhaoqiang Zheng received his BSc degree in Hunan University (2011) and PhD degree in Sun Yat-sen University (2017). Then, he joined the School of Materials and Energy, Guangdong University of Technology and currently is an associate professor. His research interests are the design, synthesis and photodetection applications of novel 2D materials and their heterostructures.

Jingbo Li received his PhD degree from the Institute of Semiconductors, Chinese Academy of Sciences (2001). Then, he spent six years at Lawrence Berkeley National Laboratory. From 2007 to 2019, he worked as a professor at the Institute of Semiconductors, Chinese Academy of Sciences. Since 2019, he has been a professor and the dean of the Institute of Semiconductors, South China Normal University. His research interests include the design, fabrication, and application of novel nanostructured semiconductors.

自组装制备$In_2Se_3/SnSe_2$异质结构阵列来抑制暗电流和增强对弱信号的响应

郑照强[1,2], 陈培峰[1], 陆健婷[1], 姚健东[3*], 招瑜[1], 张梦龙[4], 郝明明[1], 李京波[4,5*]

摘要 基于层状材料的范德华(vdWs)异质结构在下一代光电器件中显示出巨大潜力. 迄今为止, 基于堆叠或外延生长技术, 已有多种vdWs异质结构被研究. 然而, 由于vdWs异质结的合成过程复杂, 难以大规模集成异质结构器件阵列, 对其实际应用造成了极大的限制. 本文中, 我们通过脉冲激光沉积技术自组装制备了面外垂直$In_2Se_3/SnSe_2$异质结构的平面光电探测器阵列, 利用垂直内建电场来抑制暗电流并分离光生载流子. 所构建的器件具有6.3 pA的超低暗电流, 8.8×10^{11} Jones的高检测率和超过3×10^4的高信噪比. 这些性能指标不仅比纯In_2Se_3器件高一个数量级, 还展示了探测微弱信号的独特优势. 另外, 该异质结构光电探测器阵列也可以构建在柔性聚酰亚胺衬底上, 制备柔性器件. 这些器件同样显示出有效的光电探测能力, 即使弯曲200次后, 光响应仍保持不变. 这些发现为下一代大面积和高集成度光电技术的发展奠定了基础.

